Article

Chinese Science Bulletin

Materials Science

March 2012 Vol.57 No.8: 927–934
doi: 10.1007/s11434-011-4947-4

Effects of silty sand on CO_2 corrosion behavior of low-Cr tubing steel

YAN Wei[1], DENG JinGen[1*], LI XiaoRong[1], DONG XingLiang[2] & ZHANG ChunYang[2]

[1] *State Key Laboratory of Petroleum Resource and Prospecting, China University of Petroleum, Beijing 102249, China;*
[2] *China National Offshore Oil Company, Beijing 100600, China*

Received April 26, 2011; accepted August 31, 2011; published online January 6, 2012

An experimental study was carried out to assess the effects of silty sand on the CO_2 corrosion behavior of 1 wt% Cr (1Cr) and 3 wt% Cr (3Cr) tubing steel under 0.5 MPa CO_2 at 100°C and 1.5 m/s flow velocity. The 1Cr and 3Cr specimens both suffered general corrosion, but the surface was coarser in the pure CO_2 corrosion environment. Under silty sand conditions, severe pitting corrosion occurred on the 1Cr specimens and some acicular pitting appeared on the 3Cr specimens. The average corrosion rates of 1Cr and 3Cr steels increased by factors of 3 and 1.6, respectively. The corrosion products were analyzed by scanning electron microscopy (SEM), energy dispersive spectroscopy (EDS), X-ray diffraction (XRD), and electrical impedance spectroscopy (EIS). The results show that silty sand acts as an inclusion in corrosion product films and reduces the homogeneity and density of the products, rather than abrading the corrosion film. Ion-diffusion channels may build up around the irregular silty sand; this would degrade the protective capabilities of the product films and aggravate corrosion.

low-Cr tubing steel, CO_2 corrosion, silty sand, ion-diffusion channel

Citation: Yan W, Deng J G, Li X R, et al. Effects of silty sand on CO_2 corrosion behavior of low-Cr tubing steel. Chin Sci Bull, 2012, 57: 927–934, doi: 10.1007/s11434-011-4947-4

CO_2 corrosion is a severe problem in the oil and gas exploration and production industries. Many major oil companies suffer significant economic losses as a result of damage to tubing and casings caused by CO_2 corrosion; such damage can lead to well workover, production stoppages, and well shutdown. High pressure in wellheads caused by inner casing corrosion failure is a threat to workers' safety [1–3]. Since CO_2 corrosion in oil fields was first reported in the 1940s, a number of studies of CO_2 corrosion of oil and gas tubing have been conducted. These studies have focused on three aspects: the mechanism, rules, and influencing factors in CO_2 corrosion; the physical and chemical properties of the CO_2 corrosion products film; and anti-corrosion methods. Using the Cr-content steel is an effective method for resisting CO_2 corrosion, and 13Cr martensitic stainless steels have been widely studied and used in the oil and gas production industries. In the second half of the 1990s, low-Cr-content steels (0.5 wt% Cr to 5 wt% Cr) were studied extensively because of their price advantages [4–6]. According to previous research [7–9], Cr enrichment of the corrosion products is the main reason for the effective corrosion resistance of low-Cr steels. Low-Cr-bearing steels have been widely used in the oil and gas production industries, because of their effective corrosion resistance and price advantages [10,11].

When there are sand particles in the corrosive fluid, the corrosion mechanism will be much more complicated because of the synergistic effects of CO_2 corrosion and sand erosion. Many investigations have been carried out on this topic. Neville et al. [12] studied the CO_2 corrosion behaviors of carbon steel and stainless steel in a solid-liquid flow with 200–425 μm sand. He believed that sand can abrade the product film and lead to severe pitting corrosion on carbon steel. Although there was less damage on 13Cr martensitic stainless steel than on carbon steel, some pits also appeared on its surface. Rincon et al. [13] studied the CO_2

*Corresponding author (email: dengjingen@126.com)

corrosion behavior of carbon steel in multiphase flow with 150 μm sand. The results revealed that sand can increase the corrosion rate by a factor of 2–4. Lin et al. [14] studied the abrasion performance of N80 steel in water/sand two-phase flow and concluded that the damage to corrosion films caused by large sand particles is more serious than that caused by small particles. Malka et al. [15] investigated the combined effects of erosion-corrosion of AISI 1018 steel in NaCl solution. The sand size was 275 μm. He found that the corrosion rate under erosion-corrosion conditions is twice that in a sand-free environment. This is because localized disturbance increases the corrosion rate and makes the corrosion surface coarser. Stack et al. [16] studied the abrasion-corrosion behavior of X52 steel in oil/water with 600–710 μm sand. The results showed that the specimens lose weight because the synergistic effects of abrasion and corrosion are 3 and 1.4 times those of pure abrasion and pure corrosion, respectively, and severe localized corrosion occurs in the synergistic environment. The above studies are mainly based on the mechanism of sand particle abrasion of corrosion products, and the size of the sand is generally larger than 150 μm.

During oil production, although some sand-control measures for low or medium consolidated sand formation will be adopted in the overall design, silty sand (10–50 μm [17]) will still enter the wellbore along with the fluid flow; this affects CO_2 corrosion. It is therefore important to investigate the influence of silty sand on CO_2 corrosion.

Based on the investigations described above, the objective of this paper is to discuss the influence of silty sand on the CO_2 corrosion behaviors of tubing steels bearing 1 wt% Cr and 3 wt% Cr. The results are of major significance for tubing material selection in weak consolidated sandstone reservoirs with CO_2 corrosive gas.

1 Experimental

1.1 Materials

The materials used in this study were tubing steels, which were supplied by Tianjin Pipe Group Corporation, Tianjin, China, containing 1 wt% Cr and 3 wt% Cr (hereinafter referred to as 1Cr and 3Cr, respectively). The chemical compositions of the materials used in this study are shown in Table 1.

1.2 Solution

The solution used in this study is simulated oilfield water. The pH value is 6.8 and the ion concentrations are shown in Table 2.

1.3 Silty sand

The silty-sand size is from 13 to 45 μm, and was obtained using a combined sieve with 325 mesh (45 μm) and 1000 mesh (13 μm). Before the tests, the chemical compositions of the silty sand were analyzed by energy dispersive spectroscopy (EDS, FEI Quanta 200F, Hillsboro, OR, USA) and X-ray diffraction (XRD, D/MAX2500, Rigaku Corporation, Tokyo, Japan). The results show that the silty sand is mainly composed of O, Al, Si, Mg and Ca, and the chemical composition is $CaO–MgO–Al_2O_3–SiO_2$. The silty-sand concentration in the solution is 1 wt%.

Table 1 Chemical compositions of 1Cr and 3Cr (mass fraction, %)

	C	Si	Mn	P	S	Cr	Mo	Ni
1Cr	0.20	0.27	0.42	0.0089	0.00082	1.03	0.24	0.10
3Cr	0.19	0.32	0.47	0.0089	0.00082	2.93	0.39	0.17

Table 2 Oil field water ions concentration (mg/L)

K^+, Na^+	Ca^{2+}	Mg^{2+}	Cl^-	SO_4^{2-}	HCO_3^-	CO_3^{2-}
8350	3885	57	19634	850	337	0

1.4 Equipment and methods

The specimen holder of the high-temperature and high-pressure dynamic autoclave was designed by the Rock Mechanics Laboratory, China University of Petroleum, Beijing, China. The whole apparatus was made by Haianxian Oil Scientific Research Apparatus Co., Ltd., Nantong, Jiangsu Province, China, as shown in Figure 1. Coupon specimens, of width 10 mm, length 50 mm, and thickness 3 mm, were used.

Five specimens of each material were tested under the same conditions. Three specimens were used to calculate the average corrosion rate, one specimen was used for scanning electron microscopy (SEM), XRD and EDS analyses, and one was used for electrochemical tests.

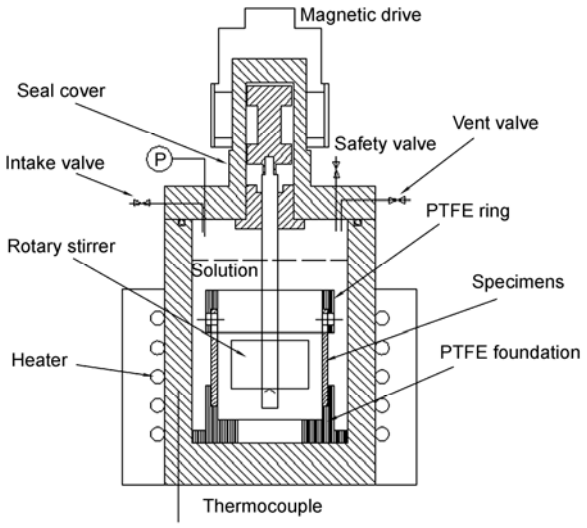

Figure 1 High-temperature and high-pressure dynamic autoclave.

The specimens were polished with silicon carbide No. 320 and No. 600 papers, rinsed with distilled water, degreased in acetone, and then weighed after drying. The specimens were mounted on a specimen holder, which was made of polytetrafluoroethylene (PTFE). The holder was placed in the autoclave, and then the simulated solution was poured into the vessel (in silty-sand-containing tests, 1 wt% silty sand was added to the solution at this stage) and the autoclave was closed. Initially, the temperature was raised to 45°C to remove some of the dissolved oxygen from the solution, and then deaeration was carried out by N_2 gas bubbling for about 2 h. After purging with N_2, CO_2 was injected into the autoclave for 5–10 min, and the temperature and pressure were raised to 100°C and 0.5 MPa. The solution was saturated with CO_2 and kept for about 0.5 h to stabilize the pressure, and then the rotary stirrer was started; the flow velocity at the specimen surface was about 1.5 m/s (rotation speed, 500 r/min). The testing time was 7 d.

The specimens were divided into three groups after the tests. The specimens in group 1 were used to calculate the average corrosion rate. First, the specimen surfaces were washed with distilled water and the corrosion products were removed by pickling in 10% hydrochloric acid solution containing an inhibitor. Then the specimens were dried and photographed (EX-H30, Casio Computer Co., Ltd., Tokyo, Japan) to record the corrosion status. Finally, the residual masses of the specimens were determined using an electronic balance (accuracy 0.1 mg) and the average corrosion rate was calculated by the weight-loss method. The specimens in group 2 were immersed in distilled water for 3–5 min to dissolve the halide crystals on the surface, soaked in acetone for 20–30 s, and dried before XRD, SEM, and EDS testing. The specimens in group 3 were cut into small pieces (10 mm in length) and welded together with a copper conductor. Then the surfaces of the welded samples, except for the corrosion surfaces, were sealed with 704 silica gel; the corrosion surfaces were prepared for the electrochemical tests.

1.5 EIS tests

Electrochemical impedance spectroscopy (EIS) plots of specimens with corrosion scale under different conditions were carried out to analyze the ion permeability of the corrosion products. The EIS measurements were performed using a three-electrode test cell (CHI660C, Shanghai Chenhua Instrument Co., Ltd., Shanghai, China). A graphite electrode was used as the auxiliary electrode, a saturated calomel electrode (SCE) was used as the reference electrode, and the test specimen was used as the working electrode (area, 1 cm^2). The glass electrolysis pool had a capacity of 500 mL. The test solution was simulated oilfield water. Before the measurements, the test solution was deoxidized for 2 h using purified N_2. The test temperature was 25°C. The EIS measurements frequency range was 10 mHz to 100 kHz, and the signal amplitude was a 5 mV sine wave.

2 Results and discussion

2.1 Surface conditions and average corrosion rate

When the samples were removed from the autoclave, corrosion product scale was found on the surface of the specimens and no scale peeled from the surface, not only under sand-free conditions, but also under silty-sand conditions. Photographs of the specimens after descaling are shown in Figure 2. In the sand-free environment, both materials suffered general corrosion, but no obvious localized corrosion such as pitting and mesa attack, and the surface was relatively coarse. However, when silty sand was added to the environment, different degrees of localized corrosion occurred on the surfaces of both materials. Severe pitting corrosion appeared on the 1Cr specimens, and the 3Cr specimens became coarser and needle-corrosion pits appeared. Figure 3 shows the average corrosion rates of the 1Cr and 3Cr steels. In the sand-free environment, the average corrosion rates of 1Cr and 3Cr were 1.0296 and 1.2254 mm/a, respectively. However, under silty-sand conditions, the average corrosion rate of the two materials increased observably to 4.1229 mm/a for 1Cr and 3.1882 mm/a for 3Cr, i.e., the rates increased by 3 and 1.6 times, respectively.

2.2 Corrosion film structure

SEM images of the 1Cr corrosion products are shown in Figure 4(a) and (b). Under sand-free conditions, the 1Cr

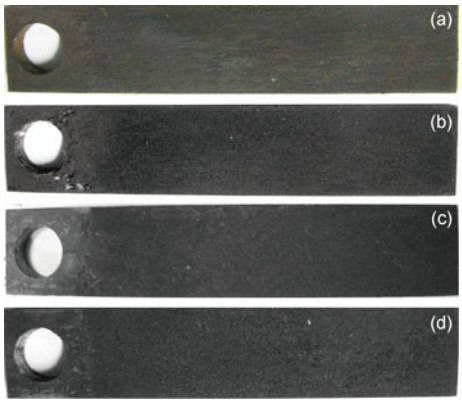

Figure 2 Appearance of specimen surfaces after descaling. (a) 1Cr, sand free; (b) 1Cr, silty sand; (c) 3Cr, sand free; (d) 3Cr, silty sand.

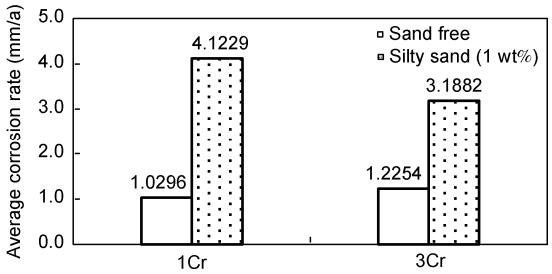

Figure 3 Average corrosion rate of 1Cr and 3Cr under sand-free and silty-sand conditions.

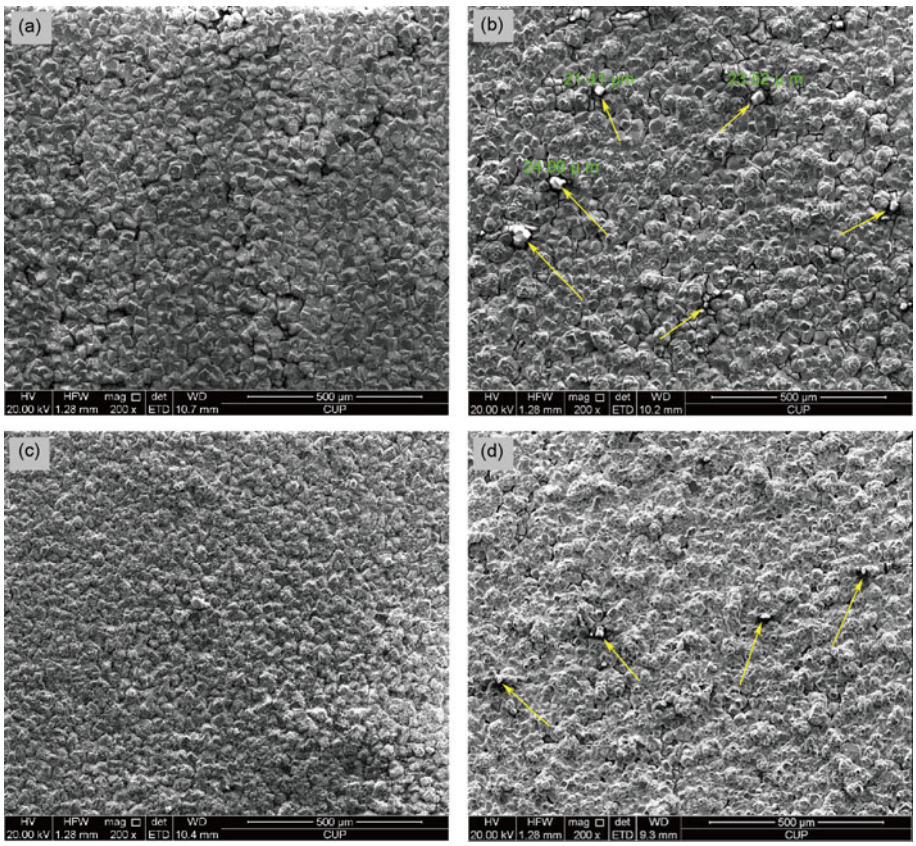

Figure 4 Surface morphologies of 1Cr and 3Cr under the two conditions. (a) 1Cr, sand free; (b) 1Cr, silty sand; (c) 3Cr, sand free; (d) 3Cr, silty sand.

corrosion product is homogeneous and the crystal particle size and color are consistent. EDS tests show that the outer scale is composed mainly of Fe, C, and O. The XRD spectra (Figure 5) and previous research [11,18] show that the main outer corrosion product of 1Cr steel is $FeCO_3$. In the silty-sand environment, the corrosion products are not smooth, and the products contain irregularly distributed bright particles. There are obvious gaps between these bright particles and the surrounding $FeCO_3$ crystals. SEM photographs of the 3Cr corrosion products are shown in Figure 4(c) and (d). Under sand-free conditions, the 3Cr surface morphology is the same as that of 1Cr, i.e., homogeneous and consistent. However, the 3Cr surface morphology changed significantly after addition of sand (Figure 4(d)). The diameter of the bright colored particles in the corrosion products is consistent with that of the silty sand used in this study and may be sand particles.

Amplified SEM images of the surface corrosion products of 1Cr and 3Cr specimens under silty-sand conditions are shown in Figure 6. It is obvious that some parts of the corrosion products are stacked, especially on the surface of the 1Cr specimens; these areas are marked in Figure 6.

The XRD spectra of the surface corrosion products on the 1Cr and 3Cr specimens are shown in Figure 5. There are no obvious differences between the compositions of the corrosion products formed under silty-sand or sand-free

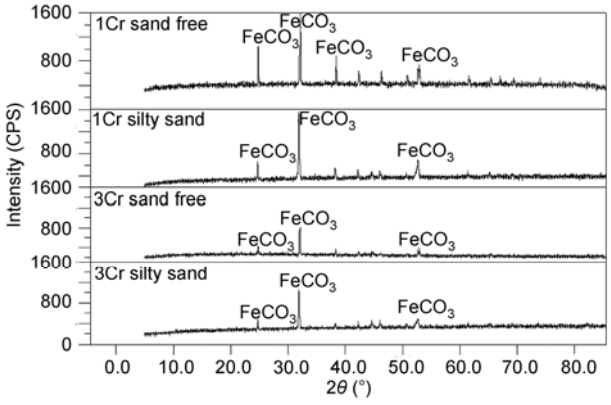

Figure 5 XRD spectra of 1Cr and 3Cr corrosion products under different conditions.

conditions; both are mainly $FeCO_3$. Amorphous Cr-enriched oxides (typical corrosion products of low-Cr-bearing steel in wet CO_2 environments [4,19,20]) data curves do not appear in the XRD spectra. This may be because the amorphous Cr-enriched oxide was covered by a thick $FeCO_3$ film.

The cross-section morphologies of the 1Cr specimen are shown in Figure 7(a) and (b). The corrosion product is uniform and thinner in the sand-free environment (Figure 7(a)), but it becomes thicker and mixed with particles under silty-

sand conditions (Figure 7(b)). The EDS analysis results for the eight test points in Figure 7 are listed in Table 3. The results show that the corrosion product consists mainly of O, Fe, and Cr (test point 1) in the sand-free environment. Under the silty-sand conditions, test point 2 should be the corrosion product, and the other particles (test points 3–6) are considered to be silty sand, because these particles have the same size and chemical composition as the silty sand.

Cross-section morphologies of the 3Cr specimen are shown in Figure 7(c) and (d). The corrosion product morphologies of 3Cr are the same as those of 1Cr under sand-free conditions and there are no irregular particles in the corrosion products. However, after addition of silty sand, some solid particles are present in the corrosion products. The EDS results show that test point 7 mainly consists of O, Fe, and Cr, and should be the corrosion product (Figure 7(c)). The solid particles in Figure 7(d) (test point 8) are the silty sand used in this study.

2.3 EIS characteristics of specimens with corrosion scale

Figure 8(a) and (b) shows the EIS plots of 1Cr and 3Cr steels with corrosion scales under the two conditions. Under

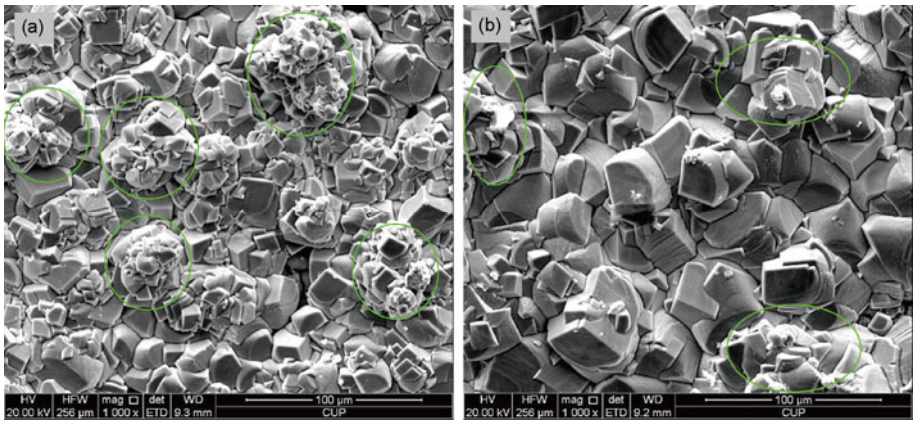

Figure 6 Surface morphologies under silty-sand conditions. (a) 1Cr; (b) 3Cr.

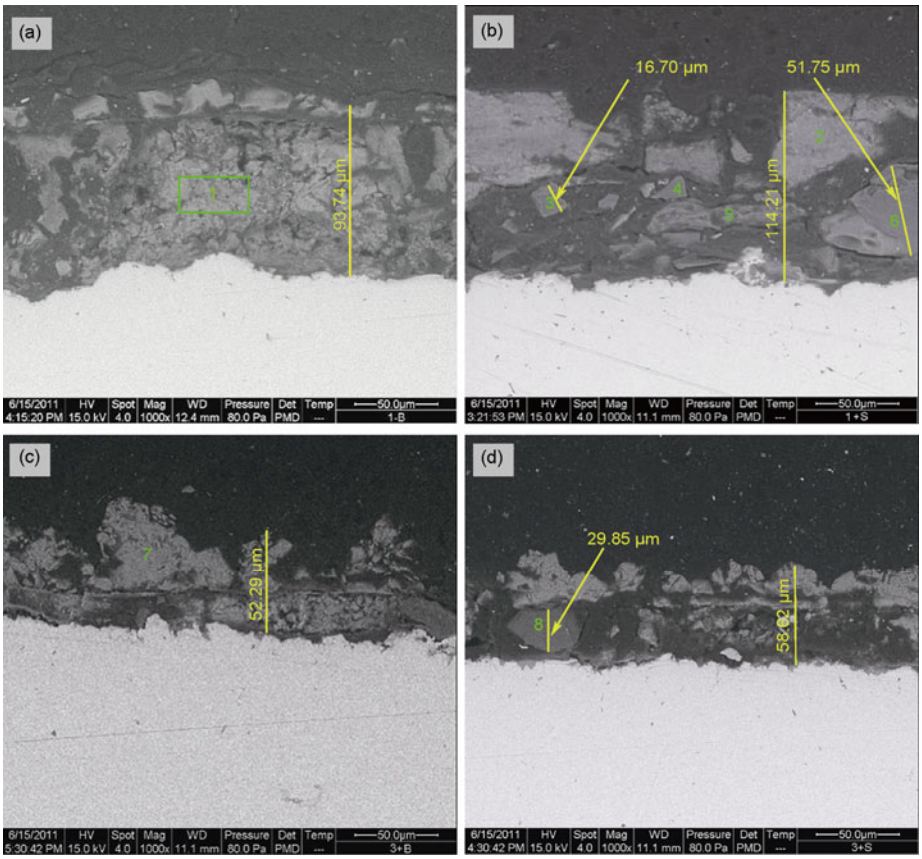

Figure 7 Cross-section morphologies of 1Cr and 3Cr steels. (a) 1Cr, sand free; (b) 1Cr, silty sand; (c) 3Cr, sand free; (d) 3Cr, silty sand.

Table 3 EDS analysis results (at%) for different points in Figure 7

Point	O	Fe	Cr	Al	Mg	Si	Ca	Speculate
1	43.64	48.87	7.49					Corrosion products
2	51.89	22.08	0.39					Corrosion products
3	54.43	10.14	1.07	1.97	17.18	1.31	14.67	Silty sand
4	52.25	5.14	0.84	39.95		1.65		Silty sand
5	38.17	11.36	1.58	5.67		43.22		Silty sand
6	43.97	8.49	0.72	46.14		0.68		Silty sand
7	46.19	39.4	10.48				1.69	Corrosion products
8	46.78	6.66		46.55				Silty sand

silty-sand conditions, for 1Cr steel, there are two time constants in the EIS results: the capacitive reactance arc in the high-frequency range and the inductance arc in the low-frequency range. The capacitive reactance arc in the high-frequency range is associated with electric double-layer capacitance and reaction transfer resistance, and the inductance arc in the low-frequency range is associated with surface activation and dissolution. The inductance arc under sand-free conditions is not obvious. This indicates that the rate of surface activation and dissolution for 1Cr under silty-sand conditions is higher than that under sand-free conditions. Moreover, from the diameter of the capacitance arc, it can be concluded that the polarization resistance of the 1Cr steel under silty-sand conditions is much less than that under sand-free conditions. All the data indicate that the corrosion film is loose and that ions can penetrate the film easily under silty-sand conditions. The film provides poor protection for the matrix.

Under sand-free conditions, the EIS results for 3Cr steel show Warburg impedance characteristics. This is because amorphous Cr-enriched oxides are produced, and these protect the base effectively. It is difficult for ions to pass through this film: therefore the electrode reaction is controlled by ion diffusion. Under silty-sand conditions, there is no Warburg impedance because sand is mixed in the film. A channel, which helps ions to pass through the film, is set up along the boundary between the sand and the corrosion film. Under these conditions, the electrode reaction is not controlled by ion diffusion and the corrosion rate increases significantly.

2.4 Mechanism of scale formation

The analysis results described above reveal that silty sand does not abrade the corrosion film, but mixes with the corrosion products. According to previous research [19–22], the main anodic reactions of low-Cr steel in CO_2-containing aqueous solution can be represented by the following four reactions:

$$Fe \rightarrow Fe^{2+} + 2e, \quad (1)$$

$$Fe + HCO_3^- \rightarrow FeCO_3 + 2e + H^+, \quad (2)$$

$$Fe + CO_3^{2-} \rightarrow FeCO_3 + 2e, \quad (3)$$

$$Cr + 3OH^- \rightarrow Cr(OH)_3 + 3e. \quad (4)$$

In view of the experimental results, the anodic reactions, and previous research [23–25], the formation of the CO_2 corrosion film on low-Cr tubing steel in a silty-sand-containing environment is explained as follows. The inner $FeCO_3$ film is generated by the chemical reaction of CO_3^{2-}, HCO_3^-, and Fe^{2+}, i.e., eqs. (2) and (3), and Fe^{2+} is generated by hydrolysis of the metal matrix (eq. (1)). This chemical process is very rapid and the film is very thin, so it has little restraining effect on further diffusion of Fe^{2+}. There is little

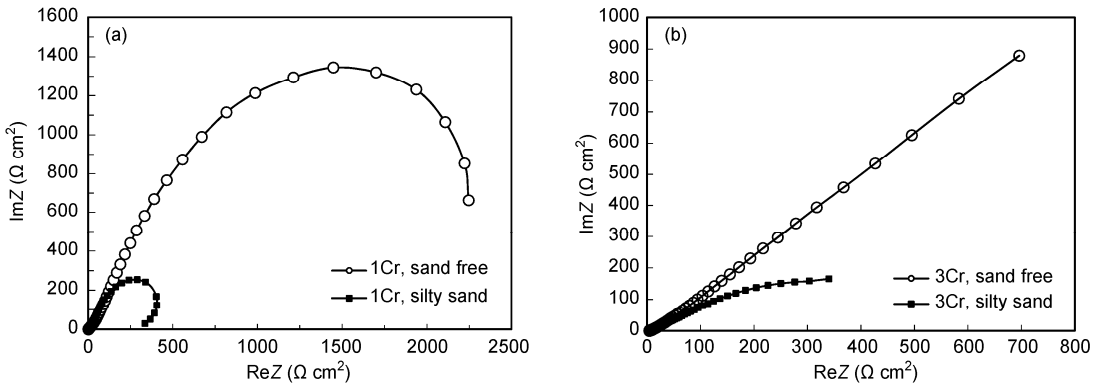

Figure 8 EIS plots of specimens with corrosion scale under the two conditions. (a) 1Cr; (b) 3Cr.

mixing of silty sand with this film, because the film grows from the matrix surface to the outer surface. In carbon steels containing Cr, another anodic reaction could occur, shown in eq. (4), and an amorphous Cr-enriched-oxide ($Cr(OH)_3$) could be detected in the corrosion products. This film is formed by deposition, so silty sand particles may be entrained in this layer, and the product will consist of $Cr(OH)_3$, $FeCO_3$, and silty sand. When the environment is sand free, Cr complexes in this film can effectively reduce the ion-exchange and corrosion rates. However, when silty-sand particles are entrained in the film, because of the different properties and irregular shapes of the silty sand in the corrosion products, ion-diffusion channels will form around the sand particles, and this significantly reduces the protective ability of the amorphous Cr-enriched-oxide film. Fe^{2+} generated from the anodic reaction will diffuse to the scale surface through the ion channels. When $[Fe^{2+}]$ and $[CO_3^{2-}]$ exceed the $FeCO_3$ solubility product, $FeCO_3$ will be deposited on the outer surface of the scale and form a loose film. This film covers the outer surface of the mixed-products scale and has weak protecting abilities. Because of the presence of the ion-channel, an area of high Fe^{2+} concentration will form around the silty-sand particles. It is therefore easy to form $FeCO_3$ stacks around the sand particles. If the sand particle size is small, the particles will be buried by the $FeCO_3$ crystals and form piles, as shown in Figure 6. On the other hand, large sand particles will crop out of the corrosion products film, as shown by the arrows in Figure 4. Based on these results, the CO_2 corrosion film structure of low-Cr tubing steel in a silty-sand-containing environment is suggested to be that shown in Figure 9.

3 Conclusions

(1) The effects of silty sand on the CO_2 corrosion behaviors of low-Cr-bearing steels in simulated oilfield water were investigated. The presence of entrained silty sand increased the alloy's average corrosion rate significantly, by a factor of 3 for 1Cr and of 1.6 for 3Cr, compared with the rates in a sand-free environment. Pitting corrosion was only observed in the silty-sand-containing environment.

(2) Silty sand mixed with the corrosion films will reduce the homogeneity and density of the corrosion film and loosen the corrosion film. Corrosion products will stack easily around the silty-sand particles.

(3) Under conditions simulating those in a down-hole environment, silty sand does not abrade the corrosion products film, but acts as an inclusion in the products. Ion-diffusion channels may form around the silty sand and the amorphous Cr-enriched-oxide film, which has good protective abilities, loses its ion-selective permeability. Ultimately, the protective abilities of the produced film deteriorates, which will significantly increase corrosion.

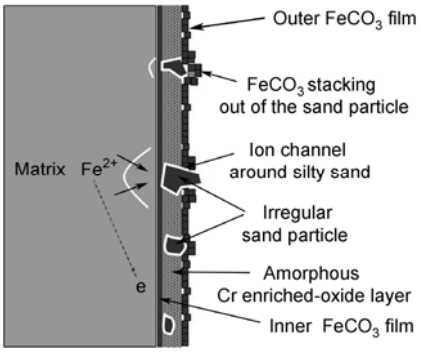

Figure 9 Corrosion film structure of low-Cr tubing steel in CO_2 and silty-sand-containing environment.

This work was supported by the National Science and Technology Major Project of China (2008ZX05024).

1 Choi H J. Material selection for smart well completions in conjunction with expandable casing technology. SPE J, 2009, 126090
2 Lu M X, Bai Z Q, Zhao X W, et al. Actuality and typical cases for corrosion in the process of extraction, gathering, storage and transmission for oil and gas (in Chinese). Corros Prote, 2002, 23: 105–113
3 Kinsella B, Tan Y J, Bailey S. Electrochemical impendence spectroscopy and surface characterization techniques to study carbon dioxide corrosion product scales. Corrosion, 1998, 54: 835–842
4 Takabe H, Ueda M. The formation behavior of corrosion protective films of low Cr bearing steels in CO_2 environments. Corrosion, 2001, 01066
5 Schmitt G, Engels D. SEM/EDX analysis of corrosion products for investigation on metallurgy and solution effects in CO_2 corrosion. Corrosion, 1988, 149
6 Chen C F, Lu M X, Zhao G X, et al. Characteristics of CO_2 corrosion scales on well tube steels N80 (in Chinese). Acta Metall Sin, 2002, 38: 411–416
7 Kermani M B, Gonzales J C, Turconi G L, et al. Development of superior corrosion resistance 3%Cr steels for downhole application. Corrosion, 2003, 03116
8 Nyborg R, Dugstad A. Mesa corrosion attack in carbon steel and 0.5% chromium steel. Corrosion, 1998, 29
9 Chen C F, Lu M X, Chang W, et al. The ion passing selectivity of CO_2 corrosion scale on N80 tube steel. Corrosion, 2003, 03342
10 Kermani M B, Morshed A. Carbon dioxide corrosion in oil and gas production—A compendium. Corrosion, 2003, 59: 659–683
11 Nice P I, Takabe H, Ueda M. The development and implementation of a new alloyed steel for oil and gas production wells. Corrosion, 2000, 00154
12 Neville A, Wang C. Study of the effect of inhibitor on erosion-corrosion in CO_2-saturated condition with sand. SPE J, 2008, 114081
13 Rincon H E, Shadley J R, Rybicki E F, et al. Erosion-corrosion of carbon steel in CO_2 saturated multiphase flows containing sand. Corrosion, 2006, 06590
14 Lin G F, Zhen M S, Bai Z Q, et al. Wear behavior of CO_2 corrosion scales on well tube steel N80 in water-sand two-phase fluid medium (in Chinese). Tribology, 2005, 1: 78–81
15 Malka R, Nesic S, Gulino D A. Erosion-corrosion and synergistic effects in disturbed liquid-particle flow. Wear, 2007, 262: 791–799
16 Stack M M, Abdulrahman G H. Mapping erosion-corrosion of carbon steel in oil exploration conditions: Some new approaches to characterizing mechanisms and synergies. Tribol Int, 2010, 43: 1268–1277
17 Yang S L, Wei J Z. Petrophysics (in Chinese). Beijing: Petroleum Industry Press, 2004. 107
18 Zhang G A, Lu M X, Wu Y S. Morphology and microstructure of CO_2 corrosion scales (in Chinese). Chin J Mater Res, 2005, 5: 537–548
19 Wang X F, Dong Z J, Liang Y J, et al. Development of economic

steels with low Cr content for anti-corrosion oil tube (in Chinese). Corros Sci Protect Tech, 2006, 18: 436–439
20 Chen C F, Zhao G X, Yan M L, et al. Characteristics of CO_2 corrosion scales on Cr-containing N80 steel (in Chinese). J Chin Soc Corros Protect, 2002, 22: 335–338
21 Takabe H, Ueda M. The relationship between CO_2 corrosion resistance and corrosion products structure on carbon and low Cr bearing steels. Corros Eng, 2007, 56: 514–520
22 Cai Y D, Guo P C, Liu D M, et al. Comparative study on CO_2 corrosion behavior of N80, P110, X52 and 13Cr pipe lines in simulated stratum water. Sci China Technol Sci, 2010, 53: 2342–2349
23 Li C F, Zhang Y, Wang B, et al. Advances in the research of CO_2 corrosion films in oil and gas production (in Chinese). Corros Prote, 2005, 10: 443–447
24 Liang M H, Zhao G X, Feng Y R, et al. CO_2 corrosion behaviors of KO110 and 3Cr110 steels (in Chinese). Corros Prote, 2005, 6: 240–243
25 Takabe H, Ueda M. The formation behavior of corrosion protective films of low Cr bearing steels in CO_2 environments. Corrosion, 2001, 01066